

The effect of soil moisture perturbations on Indian Monsoon Depressions in a numerical weather prediction model

Article

Published Version

Creative Commons: Attribution 4.0 (CC-BY)

Open Access

Hunt, K. M. and Turner, A. G. (2017) The effect of soil moisture perturbations on Indian Monsoon Depressions in a numerical weather prediction model. *Journal of Climate*, 30 (21). pp. 8811-8823. ISSN 1520-0442 doi: <https://doi.org/10.1175/JCLI-D-16-0733.1> Available at <https://centaur.reading.ac.uk/67424/>

It is advisable to refer to the publisher's version if you intend to cite from the work. See [Guidance on citing](#).

To link to this article DOI: <http://dx.doi.org/10.1175/JCLI-D-16-0733.1>

Publisher: American Meteorological Society

All outputs in CentAUR are protected by Intellectual Property Rights law, including copyright law. Copyright and IPR is retained by the creators or other copyright holders. Terms and conditions for use of this material are defined in the [End User Agreement](#).

www.reading.ac.uk/centaur

CentAUR

Central Archive at the University of Reading

Reading's research outputs online

The Effect of Soil Moisture Perturbations on Indian Monsoon Depressions in a Numerical Weather Prediction Model

KIERAN M. R. HUNT

Department of Meteorology, University of Reading, Reading, United Kingdom

ANDREW G. TURNER

NCAS-Climate, and Department of Meteorology, University of Reading, Reading, United Kingdom

(Manuscript received 10 October 2016, in final form 27 July 2017)

ABSTRACT


Indian monsoon depressions (MDs) are synoptic-scale cyclonic systems that propagate across peninsular India three or four times per monsoon season. They are responsible for the majority of rainfall in agrarian north India, so constraining precipitation estimates is of high importance. Here, a case study from August 2014 is used to explore the relationship between varying soil moisture and the resulting track and structure of an incident MD using the Met Office Unified Model. This case study is chosen with the view to increasing understanding of the general impact of soil moisture perturbations on monsoon depressions. It is found that increasing soil moisture in the monsoon trough region results in deeper inland penetration and a more developed structure—for example, a warmer core in the midtroposphere and a stronger bimodal potential vorticity core in the mid-to-lower troposphere—with more precipitation, and a structure that in general more closely resembles that found in depressions over the ocean, indicating that soil moisture may enhance the convective mechanism that drives depressions over land. This experiment also shows that these changes are most significant when the depression is deep and negligible when it is weakening. Increasing soil moisture in the sub-Himalayan arable zone, a region with large irrigation coverage, also caused deeper inland penetration and some feature enhancement in the upper troposphere, but no significant changes were found in the track heading or lower-tropospheric structure.

1. Introduction

Indian monsoon depressions (MDs) are synoptic-scale systems that usually originate in the Bay of Bengal and propagate northwestward across the Indian subcontinent, with a mean duration of 4–6 days, and an average frequency of between two and four per summer (Boos et al. 2015; Hunt et al. 2016a). Their spinup mechanism remains uncertain (Cohen and Boos 2016), although it appears likely that convective instability of the second kind (CISK; Charney and Eliassen 1964) plays at least some role (Shukla 1978); however, their primary propagation mechanism has been well

described, albeit fairly recently (Boos et al. 2015; Hunt and Parker 2016), as a coupling of horizontal nonlinear advection of the midtropospheric potential vorticity maximum and an image vortex interaction of the lower-tropospheric PV maximum with the no-normal-flow condition imposed by the Himalayas.

It also remains unclear what synoptic variables, if any, control the duration and ultimate dissipation of MDs; there is some evidence that a contemporaneous monsoon flood year or active spell tends to extend the duration of depressions in the north of the peninsula (Krishnamurthy and Shukla 2007; Krishnamurthy and Ajayamohan 2010), although this has not yet been disentangled into a primarily synoptic or mesoscale (troposphere or land surface conditions, respectively, favorable for longer duration) theoretical framework.

 Denotes content that is immediately available upon publication as open access.

Corresponding author: Kieran M. R. Hunt, k.m.r.hunt@reading.ac.uk



This article is licensed under a [Creative Commons Attribution 4.0 license](http://creativecommons.org/licenses/by/4.0/) (<http://creativecommons.org/licenses/by/4.0/>).

Nevertheless, recent work has shown that favorable conditions (e.g., higher vorticity and more moisture) at both scales is correlated with increased MD activity, duration, or intensity; for example, for soil moisture by Chang et al. (2009) and Kishtawal et al. (2013), and for the active phase of the monsoon by Hunt et al. (2016a).

Eltahir (1998) was the first to provide a solid theoretical pathway to accompany the long-held assertion that an increase in large-scale soil moisture induces enhanced precipitation. He proposed that the drops in surface albedo and Bowen ratio caused by wetting soil work to increase the near-surface specific moist static energy and boundary layer moist static energy gradient, which results in more favorable conditions for precipitation. If, however, this is to be an important process in MDs, it is likely to be indirect [it must also overcome a negative feedback at the MD center; the associated lower-tropospheric cold core (Godbole 1977; Hunt et al. 2016a) acts to cool the surface and increase stability there]; the area of maximum precipitation is found to the southwest of the center (e.g., Ramanathan and Ramakrishnan 1933) where the (adiabatic) quasigeostrophic omega equation (e.g., Holton and Hakim 2013) predicts the greatest ascent associated with the balanced MD vortex will be (Boos et al. 2015). In contrast, the Bowen ratio tends to reach a minimum just ahead (northwest) of the center (Hunt et al. 2016a). To elucidate this, following Hunt et al. (2016a), Fig. 1 shows the mean Bowen ratio (ERA-Interim, hereinafter ERA-I; Dee et al. 2011) and precipitation (TRMM; Kummerow et al. 1998; Huffman et al. 2010) for a 34-depression composite in which location and orientation are normalized such that the center lies at the origin and the heading is up the page; land-only data were used. As asserted, there is not much spatial similarity between the extrema of precipitation and Bowen ratio, indicating that if we are to believe previous work suggesting a link between MD behavior and underlying soil moisture, it may be a more subtle feedback, or work on a finer spatial scale, than that suggested by Eltahir (1998). The caveat here is that surface fluxes are an entirely modeled product in ERA-I, and so have substantial uncertainty; however, this is at least partially addressed by the similarity of composite MD precipitation between ERA-I and TRMM, and the fact that most rainfall near the center of a depression is stratiform in nature (Hunt et al. 2016b). To date, a number of studies have shown that assimilation of soil moisture, or better initial representation of it, improves the forecast of monsoon depressions in mesoscale models (Vinodkumar et al. 2007, 2008; Rajesh and Pattnaik 2016). Further, it has been shown that inland soil moisture is capable not only of extending the duration of tropical cyclones (Andersen and Shepherd 2017), but in some cases of allowing them to reintensify (Kellner et al. 2012).

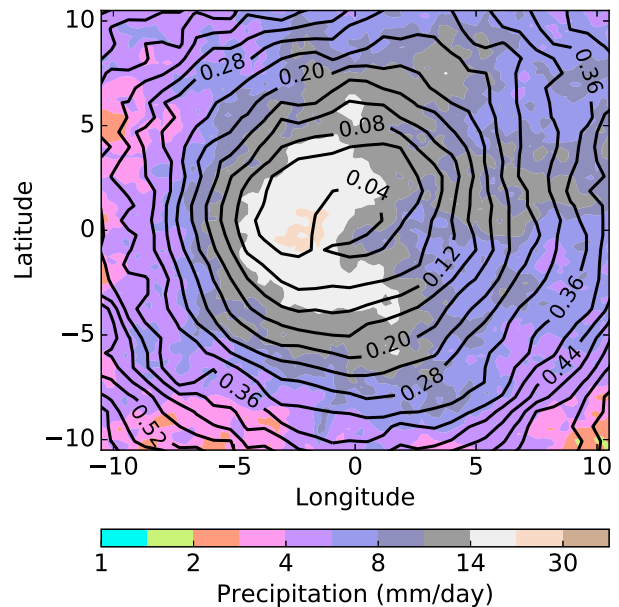


FIG. 1. Bowen ratio (contours) and precipitation (colors) for a 34-depression composite (1998–2014), as described by Hunt et al. (2016a); the composite is normalized such that the center of each depression is placed at the origin, and each is rotated so that the heading is up the page. For both fields, only points over land were composited.

Soil moisture is one of the meteorological variables subject to greatest change with respect to the progression of the Indian monsoon, largely due to its correlation with accumulated precipitation. The NOAA CPC reanalysis soil moisture climatology (Van den Dool et al. 2003) and the ESA Climate Change Initiative (CCI) satellite-derived soil moisture climatology (Liu et al. 2011, 2012; Wagner et al. 2012) for India for April, June, August, and September are given in Figs. 2a and 2b, respectively, and show a clear northwestward advance through most of the season: some areas in the monsoon trough have September soil moisture more than double that of June. Naïvely, then, we might expect MD tracks to penetrate deeper inland later into the monsoon season, given the expected influence of antecedent soil moisture on the development of MDs. Figure 3 shows the mean MD track for each month (1979–2015) from the track datasets of Hunt et al. (2016a) and Hurley and Boos (2015) respectively; note that the MD tracks have been extended to include parts where the depression is strictly in a monsoon low regime (that is to say, the surface winds are below 8.5 m s^{-1}). There is some weak evidence here to suggest that not only do MDs tend to progress farther inland later in the season, they also seem more likely to have overland genesis. This should be taken with the caveat that large-scale conditions over the subcontinent also clearly play some part, given that

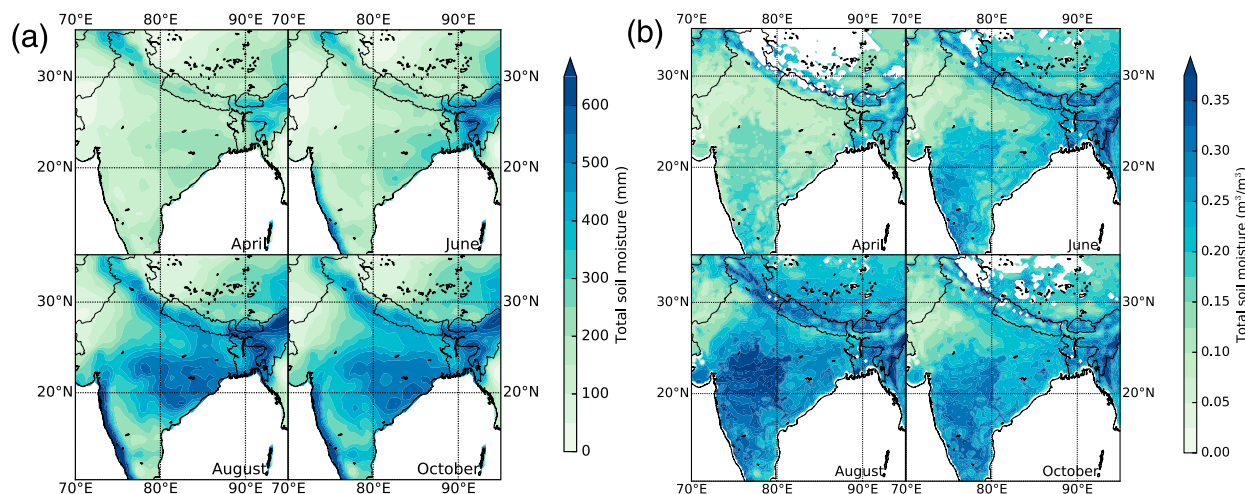


FIG. 2. Monthly soil moisture climatologies for the Indian subcontinent from two products: (a) NOAA CPC reanalysis total soil moisture (data provided by the NOAA/OAR/ESRL Physical Sciences Division (PSD), Boulder, Colorado, from their website at <http://www.esrl.noaa.gov/psd/>) and (b) ESA CCI satellite-derived volumetric soil moisture.

there is evidence that the September tracks start to re-cede, despite high levels of soil moisture remaining.

So, if soil moisture has some effect on the duration of MDs, which seems at least plausible, we are then faced with the secondary question of whether antecedent soil moisture patterns could affect the heading of existing MDs. Chen et al. (2005) showed that, in theory, the off-center latent heat released by the asymmetric rainfall distribution would interact with the local circulation to create a negative velocity potential southwest of the MD center, and therefore there would be some tendency for the MD to move in that direction. However, this mechanism is unlikely to be the primary one, since depressions typically move toward the northwest, rather than the southwest. Furthermore, Baisya et al. (2017) recently showed using a mesoscale model that precipitation intensity in MDs is strongly coupled with antecedent soil moisture. Two simple experiments are therefore proposed: 1) a uniform change in soil moisture across the monsoon trough region to determine the sensitivity of MD duration to antecedent land surface conditions, and 2) a uniform change in soil moisture in the highly farmed region across the Himalayan foothills (typically several hundred kilometers north of MD tracks; Roy et al. 2015) to determine to what extent MDs can be steered by soil moisture. These questions are presented in the context of an initial case study, but we hope that the results are sufficiently thought-provoking that further research on this topic will be motivated.

We will discuss the experimental setup and outline the methodology in section 2, then outline and interrogate the results, looking at contrasts in track and structure in section 3 before concluding in section 4.

2. The Met Office Unified Model and experimental setup

a. Overview and case study selection

The version of the Met Office Unified Model (UM) used for this study runs the Global Atmosphere, version

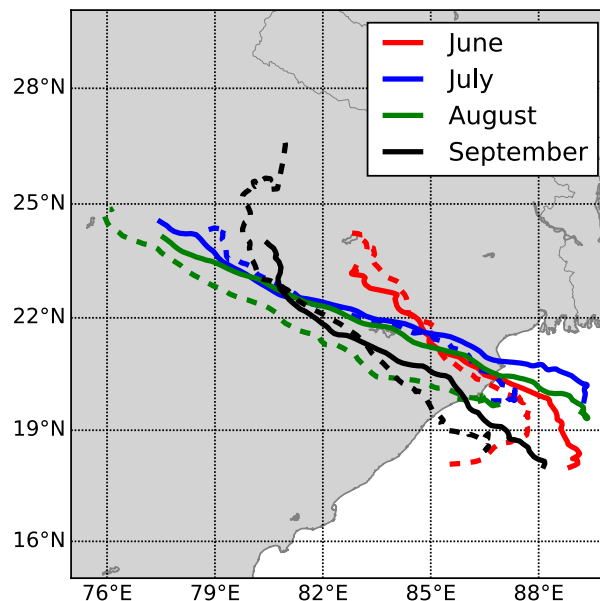


FIG. 3. Average MD tracks for each month (June through September represented by red, blue, green, and black, respectively) during the Indian monsoon. Solid lines represent mean tracks from the Hunt et al. (2016a) database and dashed lines those from the Hurley and Boos (2015) database. These tracks also include days where the disturbance is classified as a monsoon low, as well as a monsoon depression.

6.0, scheme (GA6.0; Walters et al. 2017) at N768 resolution (~ 26 km) with 85 vertical levels over a global domain; the numerical scheme is semi-implicit and semi-Lagrangian (Davies et al. 2005), and due to the resolution a number of subgrid processes are parameterized, including convection [e.g., Gregory and Rowntree (1990), with additions].

In choosing an appropriate case study to use in this experiment, we were subject to two criteria: first, and more importantly, that the MD happened within the last few years, which means that higher-resolution, better-quality analyses are available for initialization; second, that the MD had a track resembling the average for MDs (see Fig. 3) such that it could be seen as a fair representative of the spectrum of MDs incident on the east coast of the peninsula. The most suitable such event was the MD of early August 2014, which featured depression-status wind speeds from 200 km south of Kolkata until it was downgraded to a monsoon low 400 km due south of Delhi. All experiments were initialized at 0000 UTC 3 August, the day this event was declared a monsoon depression.

b. The land surface scheme and parameterization

The operational land surface model in the Met Office UM is the Joint U.K. Land Environment Simulator (JULES; Best et al. 2011). This employs the Met Office Surface Exchanges Scheme (MOSES; Cox et al. 1999; Essery et al. 2003) to handle hydrological processes, both subterranean and in the boundary layer. A brief description of the governing equations in the soil hydrology subroutine, which is taken from the relevant part of the MOSES documentation, is given in the appendix. The interaction between clouds and shortwave/longwave radiation is also handled explicitly by the prognostic cloud scheme in the UM (PC2; Wilson et al. 2008) following Edwards and Slingo (1996).

c. Ensemble generation

There are two types of stochastic perturbation that can be employed to generate a spread of forecasts in a numerical weather prediction model: uncertainties in the analysis can be represented by perturbing the initial conditions, whereas uncertainties in the model can be represented by using any number of physics perturbations (e.g., time-varying parameterizations). Operationally, the Met Office use the Met Office Global and Regional Ensemble Prediction System (MOGREPS; Bowler et al. 2008) to generate ensemble NWP runs; given that this was designed specifically for the UM, we aim to make our ensemble generation as similar as possible. MOGREPS uses two distinct stochastic physics schemes: random parameters (RP) and stochastic

kinetic energy backscatter (SKEB). The former uses the premise that many parameters in the various parameterizations in the UM are tuned to empirical values that appear to give the best representation of the relevant process, which can be periodically varied at differing frequencies between physically reasonable values to produce a spread of forecasts; the latter reintroduces kinetic energy lost through poor representation of the mechanisms by which small-scale processes cascade energy to larger scales (Shutts 2005). Initial tests suggested that using SKEB perturbations tended to artificially weaken MDs and cause them to have much shorter tracks. Thus in our study we used a stochastic perturbed tendencies (SPT) scheme that simply randomly perturbs the summation of tendencies from all parameterizations in the model (Buizza et al. 1999).

In our ensemble, we must also attempt to represent uncertainties in the analyses that are used to initialize the model. In MOGREPS this is typically done by applying an ensemble transform Kalman filter (ETKF; Bishop et al. 2001) to a previous ensemble run, assimilating observations to assess where perturbations will have the largest impact. As operational ensemble analyses were not readily available for our case study, we opted to simulate the uncertainty by adding white noise of amplitude 0.5 K to boundary layer potential temperature. Sensitivity tests determined that this gave a realistic spread of MD tracks from a short initialization without suppressing the development and progression of the depression. For each subexperiment, which are differentiated by varying soil moisture in the same region, a 10-member ensemble was used; for each ensemble member, a random seed was used such that across each experiment each ensemble was generated via the same set of pseudorandom parameters to allow intercomparability.

d. Soil moisture ancillaries

As discussed in the introduction, two case study experiments are proposed to explore the sensitivity of duration and heading respectively to underlying soil moisture. Figure 4 shows the masks used to set up the soil moisture ancillary files: the red polygon covers much of South Asia, the green polygon covers the typical monsoon trough region, and the orange covers the sub-Himalayan arable land that is becoming increasingly intensively irrigated and farmed. In each instance, the soil moisture control (perturbations to which will be used in the experiments) is the August climatology as computed from a fully coupled high-resolution climate simulation in the UM. This was chosen to reduce spinup/resolution issues that could be introduced by using a climatology from, for example, either of the

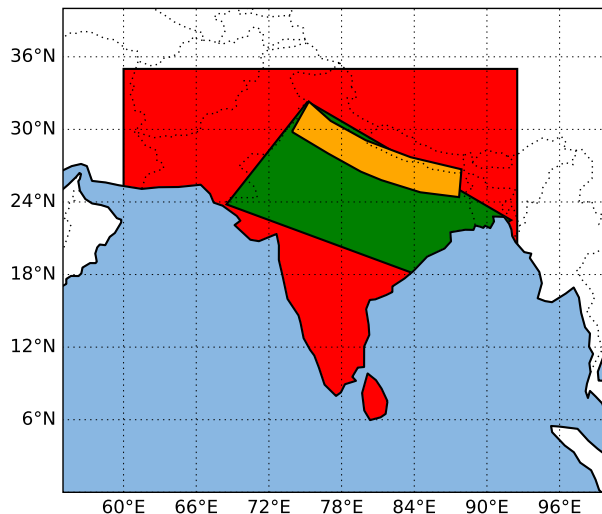


FIG. 4. Map showing the three masks used in the experiments in this study. The red box covers the entire peninsula and some of the rest of South Asia, the green box approximates the region where the monsoon trough is most active, and the orange box covers the intensively irrigated and farmed area in the Himalayan foothills.

datasets in Fig. 2. This is the current method used for soil moisture initialization of the Met Office UM in operational NWP mode.

For the first experiment (hereinafter trough zone), soil moisture in the monsoon trough region (the green polygon in Fig. 4) in which MD tracks are typically entirely embedded was altered to 1%, 80%, 100% (control), 120%, and 500% of its August climatological value. The 500% value unsurprisingly gives significant oversaturation across much of the region; where this was the case, soil moisture values at these locations were set to their saturation values. In reality, this scaling is achievable only over the dry northwest, and the average saturation value over the trough region is approximately 167%. Conversely, for the second experiment (hereinafter arable zone), soil moisture over South Asia (the red polygon in Fig. 4) is set to 1% of its August climatological value, except for inside the arable sub-Himalayan area (orange polygon) where the values were set to 1%, 50%, 100%, and 500% of the climatology. This region was traced to resemble, as much as possible, the belt of sub-Himalayan arable grassland where irrigation is becoming rapidly and increasingly prevalent (Roy et al. 2015)—the area where anthropogenic changes to the surface are likely to have the biggest impact. Values of soil moisture approaching 1% of the August climatology could be found in an extremely dry premonsoon period, but we remind the reader that the purpose of this experiment is to test the effect of soil moisture contrast in the region, not necessarily to replicate a physical event.

e. Tracking

The tracking algorithm used to determine the trajectories of MDs in output data is an updated and extended version of that described in Hunt et al. (2016a). Data at individual time steps in the output are filtered subject to the India Meteorological Department (IMD) criteria for MDs (minimum 8.5 ms^{-1} surface wind speed and two closed surface isobars at even hectopascal values) as well as some transient-filtering criteria (lower-tropospheric vorticity above $3 \times 10^{-5} \text{ s}^{-1}$; smoothed MSLP must be local minimum), and single-time-point candidates are linked together using a simple nearest-neighbor algorithm.

3. Results

a. Tracks

Tracking results from the trough zone experiment are shown in Fig. 5a. The average tracks for each subexperiment (thick, colored lines) were computed using normalized track durations for each of the 10 ensemble members; that is, points were grouped and averaged by total MD lifetime fraction rather than absolute time since genesis, with termination points for all ensemble members across the experiment given by crosses of the relevant color. The pale green area underneath is a concave hull of all points of all ensemble tracks from the control subexperiment (i.e., underlying soil moisture set at 100% of the August climatology). The official IMD track for the event is also given in black for illustration.

A first inspection of the average tracks seems to suggest that an increase in underlying antecedent soil moisture results in deeper penetration of MDs through the monsoon trough region; this is visible both in the average termination points and the individual ones. Further inspection indicates that the 500% and 120%, and 100% and 80%, average tracks are closely matched pairs, both along track and at termination. The former couple is a result of the August soil climatology already being fairly close to saturation in this region, so the difference between 20% extra moisture and saturation is fairly small. Performing Hotelling's t^2 test (Hotelling 1992)—the multidimensional generalization of the standard Student's t test for determining whether data are significantly different from each other (we have also applied Welch's generalization to allow for unequal variance in the two comparison populations; Welch 1947)—to assess whether the subexperiment ensemble terminations are distinct from each other, we find that all pairs apart from the aforementioned two are significantly different from each other at the 95% confidence level. This leads us to conclude that there is a likely

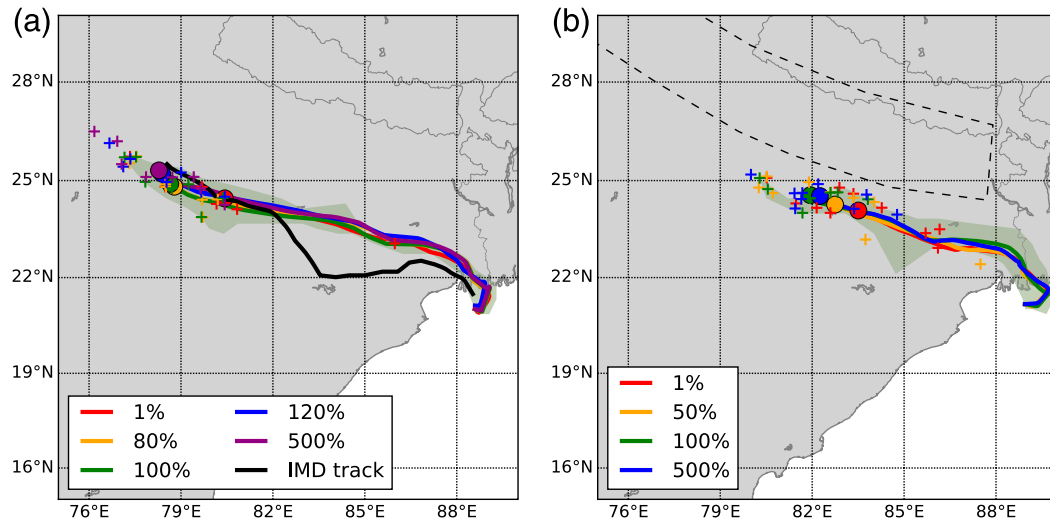


FIG. 5. Track results from varying soil moisture in (a) the monsoon trough and (b) the sub-Himalayan arable zone. For each subexperiment, the average track is given by the thick line with its termination given by the filled circles, and the individual ensemble 10-member track terminations are given by crosses of the same color. Also shown, in pale green, is a concave hull of the “100%” [for (a), this is simply the control] ensemble plume for each experiment. In (a), the official MD track from the India Meteorology Department is given by the solid black line; in (b), the border of the arable zone is denoted by the dashed black line.

causal relationship between large-scale antecedent soil moisture in the monsoon trough region, and the duration/distance traveled by incident monsoon depressions. So, is this deeper penetration due to faster inland propagation or a longer duration? Using the ensembles, we can compute the mean speeds and durations for the 1%, 80%, 100%, 120%, and 500% ensembles; the mean propagation speeds are 3.7, 3.7, 3.7, 3.9, and 3.9 m s^{-1} , with corresponding mean durations of 3.7, 4.3, 4.4, 4.2, and 4.3 days. Applying a significance test, we find that the mean ensemble speeds for the two wettest cases (500% and 120%) are significantly different from the drier ones, and that the mean duration for the driest case (1%) is significantly different from the four wetter ones.

The arable zone experiment was set up to determine to what extent moisture changes in relatively distant soil could affect the steering of a contemporaneous MD. Recall that for this experiment, the soil moisture over South Asia was set to 1% of the climatology and to the value specified (1%, 50%, 100%, or 500%) of the climatology in the sub-Himalayan belt. The results from this experiment are presented in Fig. 5b in an identical fashion to those from the trough zone experiment. In the absence of a control run, the concave hull given is for the “100%” ensemble plume. While it may seem contrived to have such extremely dry soil over almost the entire peninsula for the sake of establishing a strong contrast for our experiment, these desiccated conditions are not particularly uncommon in the preonset conditions of

late May (Fan and Van den Dool 2004) when extreme surface temperatures and scarce precipitation are usual, and depressions can still form in the Bay of Bengal (Rao and Jayaraman 1958; Mooley 1980).

An initial overview of Fig. 5b suggests two broad characteristics. First, the spread of ensemble mean terminations is smaller than in the trough zone experiment; this is almost certainly attributable to the altered soil area both having a smaller area and being further away, and thus being less influential. Second, all the average tracks are shorter than in the previous experiment, plausibly due to a larger area of desiccation than in the 1% trough zone subexperiment resulting in even less water being available over the peninsula, bearing in mind that MDs draw moisture in from distances of up to 1000 km (Hunt et al. 2016a). We also note that while there is a perfect rank correlation between soil moisture fractional change and mean termination latitude, the mean track for the 100% subexperiment is longer than that for the 500% ensemble. Repeating the termination point significance analysis carried out for the trough zone experiment, we find that the three wettest subexperiments have mean track termination points significantly different from the driest (1%), but not from each other, at a 95% confidence level.

b. Structure and evolution

Having established that soil moisture changes, both local and distant, are capable of significantly altering the

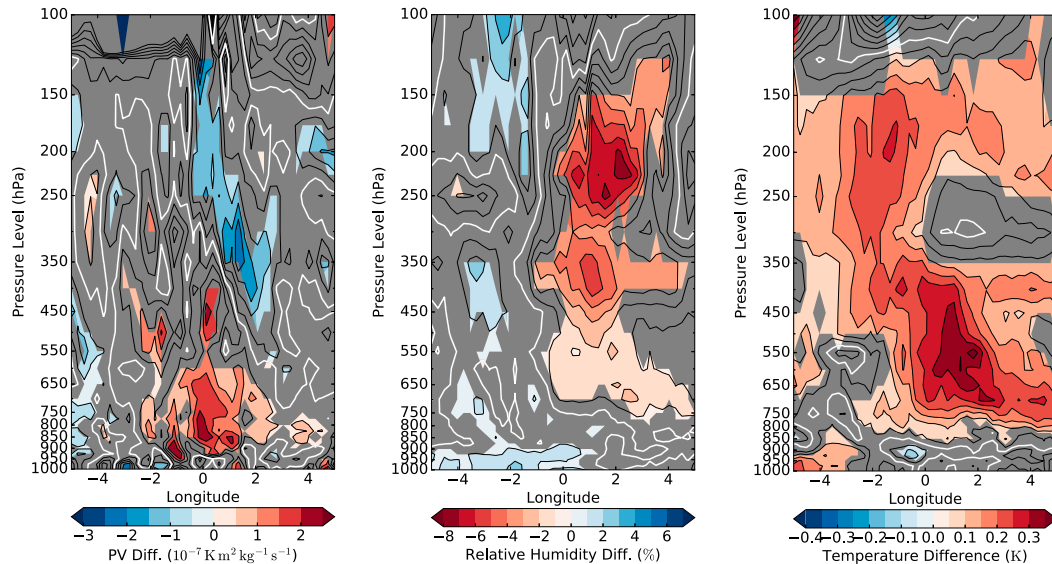


FIG. 6. Differences in selected fields of the composite mean ensembles for the 500% and 1% (the former minus the latter) trough zone experiment. The composite is normalized such that its center lies at the origin, but no rotation is carried out; these are then presented as a height–longitude cross section (at zero latitude). Greyed areas indicate the difference between the subexperiment composites was not met at the 95% significance level according to a 10 000 member bootstrap test. The selected fields are (left) potential vorticity ($10^{-7} \text{ K m}^2 \text{ kg}^{-1} \text{ s}^{-1}$), (center) relative humidity (%), and (right) temperature (K). White lines on each subfigure indicate the zero contour.

track of a passing MD, we will now examine the differing synoptic structure that these changes cause and attempt to bring the discussion to its conclusion. The largest contrast was seen in the trough zone experiment, so we shall start the discussion there. Figure 6 shows longitude–height cross sections through 500%-minus-1% composite variables from the trough zone experiment. We will briefly note here that structural changes of similar shape are found by comparing composites arising from smaller changes in soil moisture, but with varying losses in magnitude and hence significance. The center of the MD (assuming one existed) at each time point across all ensemble members for the relevant subexperiment is centered at the origin; however, unlike Fig. 1, we do not rotate these composites since the soil moisture changes introduced were anisotropic. We note that these differences are consistent across the other, nonextreme, experiments (not shown), albeit with reduced areas of significance (typically more confined to the upper troposphere) and smaller magnitudes.

We see that the composite MD for the wettest soil moisture case (in contrast to the driest) is more intense, as the midtropospheric thermal high (Godbole 1977; Hurley and Boos 2015; Hunt et al. 2016a) is markedly stronger, with accompanied strengthening of both the 700- and 500-hPa PV maxima; secondarily there is evidence of an anomalous west–east circulation with

enhanced ascent ahead of the MD center (i.e., to the west) with enhanced relative humidity there, and decreased humidity and PV in the upper troposphere behind the center; and, further, there is evidence of increased westward axial tilt with height. We would expect these effects to be associated with increased precipitation west of the center, and we see in Fig. 7a that this is indeed the case. Figure 7 gives the 500%-minus-1% horizontal composite surface precipitation and 850-hPa wind for both experiments. In the case of the trough zone experiment, we see, as expected from the previous discussion, a substantial increase (beyond 40 mm day^{-1}) in precipitation downshear (i.e., to the west) of the MD, with some slight reduction toward the east of the center; however, it is not clear whether the increase in soil moisture enhances precipitation via the Eltahir mechanism, or simply whether it allows more moisture to be inserted into the MD that then grows by other means. The 850-hPa composite difference winds are also given in this figure; they indicate the increased soil moisture sets up a large-scale, weak anomalous anticyclone that is split roughly in half, noticeably intensifying the zonal components of the MD circulation near the center, thus making the core more cyclonic. This localized feature enhancement of the MD is very similar to the behavior over ocean (Hunt et al. 2016a) where features (particularly wind) tend to have greater magnitude but smaller radial extent.

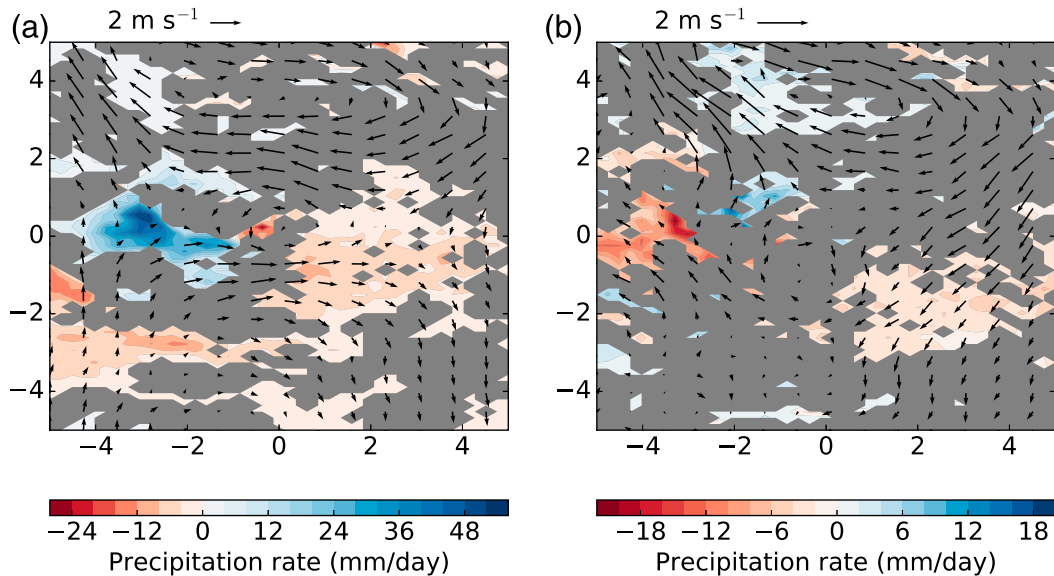


FIG. 7. Longitude–latitude cross sections of composite precipitation (mm day^{-1}) and 850-hPa winds, taken as the difference of the ensemble means for the 500% and 1% subexperiments (i.e., 500% mean minus 1% mean) of (a) the trough zone experiment and (b) the arable zone experiment. Construction and representation of significance are identical to that of Fig. 6. Note that while these composites are centered on the MD, they are not rotated.

For comparison, the equivalent figure to Fig. 7a for the arable zone experiment is Fig. 7b. Here, the consequence of increased soil moisture is largely confined to the north of the MD as expected, where a very weak anticyclone is established over the cold high associated with the wetter ground; although the effect is weaker than in the trough zone experiment, there is still an appreciable increase in the strength of the zonal circulation in the north quadrant of the MD. There is little change to the precipitation, except for a slight increase in the north over the increased soil moisture and a reduction in the west. On reflection, we should expect little difference to the large-scale structure of the MD, but the strongest contrast is likely to be meridional given the nature of our perturbation; therefore, we now consider some latitude–height cross sections for the 500%-minus-1% difference composites. These are given for potential vorticity, relative humidity, and temperature in Fig. 8. It is clear (and unsurprising) that the effect of changing arable zone soil moisture is felt substantially less by the MD than changing trough zone soil moisture, since the arable zone soil moisture perturbation is some distance from the MD core. The most prominent effect of wetting the soil there is to set up a wet, cool boundary layer; this, in turn, acts to vertically extend the warm core of the MD while slightly reducing moisture in the upper troposphere. Computation of mean CAPE (not shown) for each subexperiment suggests a slight increase around the center with increasing soil moisture. There is no real

evidence of this apparent strengthening, however, in the precipitation or lower-tropospheric wind fields; the only appreciable increase in magnitude is of the 700-hPa PV maximum.

It is also important to consider how varying soil moisture affects MDs as a function of their lifetime. For example, one would suppose the impact to be quite minimal while most of the MD is over the ocean. To test this, we can explore how selected fields from the trough experiment ensemble sets vary as a function of depression lifetime (simply a normalized time axis: 0% is the time of MD genesis, and 100% is the time of MD lysis)—this is given for four fields in Fig. 9, in which the colors red, yellow, green, and blue represent fractional changes to trough soil moisture of 1%, 80%, 120%, and 500%, respectively. Each field is computed over a box of side length 250 km centered on the MD center. The topmost field in the figure is maximum CAPE found in the quadrant of the aforementioned box that contains the next track point of the MD. There is a marked region (roughly 40%–70% through the MD lifetime) where the average maximum CAPE in all subexperiments is significantly higher than during the rest of the lifetime, and it is in this region that a change in soil moisture has the strongest effect, with the extreme subexperiments' ensemble members almost having zero overlap. We also note that here, as well as in the other fields, predictability is rapidly lost (i.e., the ensemble spread significantly widens) once the MD starts to dissipate, and

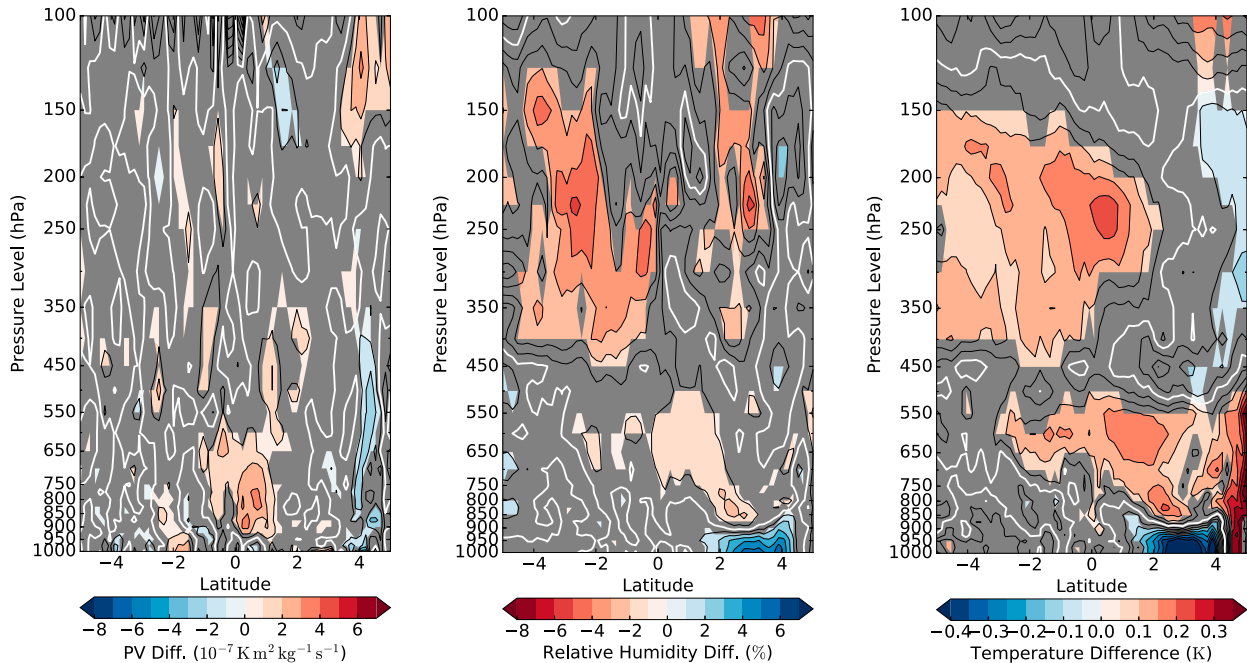


FIG. 8. Differences in selected fields of the composite mean ensembles for the 500% and 1% arable zone experiment. Construction identical to Fig. 6, except that these are latitude–height cross sections. The selected fields are (left) potential vorticity ($10^{-7} \text{ K m}^2 \text{ kg}^{-1} \text{ s}^{-1}$), (center) relative humidity (%), and (right) temperature (K). White lines on each subfigure indicate the zero contour.

further that in this regime the effect of varying soil moisture becomes negligible. In this particular instance, it is also true that during the spinup phase of the MD there is no obvious correlation between increased soil moisture and enhanced CAPE. The reader's eye may be drawn to this phase in particular both for its low CAPE and the fact that it continues to drop in all cases before it hits land. Inspection of contemporaneous reanalyses suggests that this system existed as a tropical low for a few days in the head of the Bay of Bengal (eroding CAPE), and, as can be seen from Fig. 5, remained there for a little longer thereafter (eroding it further, as seen in Fig. 9).

Related to CAPE, but not shown, is convective inhibition (CIN). Changes in soil moisture have been shown to affect CIN (e.g., Clark and Arritt 1995), which typically reaches minimum magnitude just ahead of the depression center (Hunt et al. 2016a). Applying the same analysis that we did for CAPE, we find that in the 1% case CIN is significantly much more negative (less conducive to convection) and that this extreme is much longer lasting in the vicinity of the center when compared to the other cases. The remaining cases did not differ significantly from each other.

Second from top in Fig. 9 is the mean total precipitable water in the area surrounding the MD center.

This field is less variable than CAPE but still displays a clear maximum across all subexperiments at approximately 60% of the MD lifetime before rapidly falling away. As with maximum CAPE, there is significant correlation between trough soil moisture and mean total precipitable water as well as a significant difference between the values of the extreme subexperiments during the middle period where the MD is at its strongest, followed by a complete loss of correlation, significance, and predictability after this point; however, unlike CAPE, the correlation and significance are retained during spinup. Second from bottom is the mean lower/midtropospheric temperature anomaly (averaged for 850–400 hPa); here the picture is much the same as for total precipitable water, although the correlation is no longer significant at the 95% confidence level, and the ensemble spread does not widen as much during lysis. Finally, at the bottom is maximum relative vorticity in the lower troposphere (900–800 hPa); while this is an inherently variable field, and consequently although there is arguably some correlation between it and soil moisture during the period of maximum intensity, it is not significant, nor is the difference between the two extreme subexperiments significant more than occasionally. That having been said, any semblance of correlation vanishes, as with the other fields, during the dissipation phase.

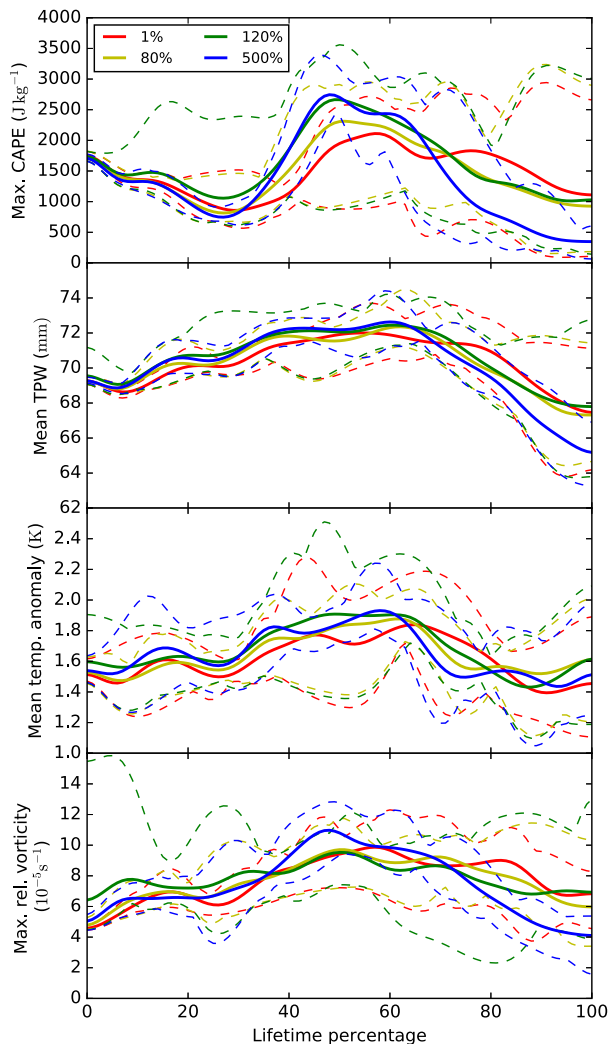


FIG. 9. Selected fields as a function of normalized depression lifetime for the trough experiment, with the soil moisture changes colored thus: 1%–red, 80%–yellow, 120%–green, 500%–blue. From top to bottom, they are the maximum CAPE (J kg^{-1}) found in the advance quadrant (see note at end of caption) of the MD; mean total precipitable water (mm); mean temperature anomaly (K) between 850 and 400 hPa; and maximum relative vorticity (10^{-5} s^{-1}). The thick solid lines represent the ensemble average, with the thinner dashed lines representing the ensemble minimum and maximum values. Each is computed over a box of side length 250 km centered on the MD center. (The quadrants are delineated into northwest, northeast, southeast, and southwest; that is, if the MD is propagating west-northwest, CAPE is computed in the northwest quadrant.)

4. Discussion and conclusions

Monsoon depressions are responsible for the majority of the precipitation incident throughout the summer across northern peninsular India and the monsoon trough region. Previous work has established the possibility of at least a correlative connection between

antecedent soil moisture and the behavior of incident MDs, but this is the first study to investigate the nature of that relationship. Soil moisture, in two key areas where it has previously been identified as variable and of meteorological importance, was varied through multiples of the climatology in a selected NWP case study run in the global Met Office Unified Model.

We have presented the results of a set of idealized sensitivity tests, each with multiple ensemble members, initialized from the analysis of a typical depression chosen in August 2014. While we have framed these tests in the context of a single MD, significant differences have emerged between the ensembles due to the imposition of soil moisture anomalies; we hope that this will motivate further study of other events to explore the climatological relationship between MDs and soil moisture.

We found that both the structure and propagation of the MD was significantly sensitive to changes in soil moisture in the monsoon trough region: wetter conditions there caused a strengthening of the MD with increased central PV and a warmer thermal core, as well as a more pronounced westward axial tilt. Such cases were also found to travel farther inland before dissipating. Further, we found that these changes were greatest (among variables associated with MD strength: CAPE, total precipitable water, midtropospheric temperature, and lower-tropospheric vorticity) during the period when the MD is most intense, and that varying soil moisture has no noticeable effect on the MD during its spindown.

In the other experiment, soil across South Asia was kept desiccated while moisture in the sub-Himalayan arable zone was varied. This had a lesser effect on both the structure and track of the case study, although some significant differences persisted: tracks in the wetter cases terminated later, and there was some weak strengthening of the MD in the middle and upper troposphere.

We also noted that in the wetter trough zone experiments, the ensemble composite MD became more axially confined (as well as more intense), mimicking MD behavior over the ocean (Hunt et al. 2016a). This suggests that added soil moisture in this region provides more moisture to the lower troposphere and subsequently enhances convective activity related to the MD. This is further enhanced by increased lower-level convergence to the west of the center.

This leaves us with several questions for further study. First, how exactly does a monsoon depression interact with the boundary layer? It has been indicated both here and in previous work that MDs are very efficient at moving water from the surface through the PBL and into

the troposphere, despite not having particularly high wind speeds (by definition MDs lie at between 5 and 7 on the Beaufort scale). This could be appropriately investigated by examination of a case study in a mesoscale-resolution NWP model. Second, how would an incident MD respond to horizontal gradients in soil moisture, rather than the block changes performed in this study [e.g., with increasing (and decreasing) values both along track and across track]? Third, even though we have spoken of CISK as the energy source for MDs, the precise role of CISK, and its magnitude, remains uncertain. Uncovering the true MD spinup mechanism would provide invaluable direction for future research on the topic, and could be investigated using mechanism-denial experiments in a suitable NWP framework (cf. Craig and Gray 1996).

Acknowledgments. KMRH received partial support from the Met Office under the aegis of the NERC CASE studentship scheme, and was also supported by the NERC Grant NE/L501608/1. KMRH wishes to thank Paul Earnshaw and David Walters at the Met Office for their untiring assistance with setting up the UM. KMRH also wishes to thank Christopher Taylor at CEH for helpful discussions regarding soil moisture. A. G. Turner was supported by the INCOMPASS project (NERC Grant NE/L01386X/1).

APPENDIX

Overview of the Land Surface Scheme Used in the Model

Four soil layers are used, for both the thermodynamic and hydrological subroutines, at depths from the surface of 10, 25, 65, and 200 cm, respectively; the prognostic total soil water in each layer is given by

$$M = \rho_w \Delta z \Theta_u, \quad (\text{A1})$$

where ρ_w is the density of water, Δz is the thickness of the layer, and Θ_u is the liquid water concentration (for the sake of this discussion, we neglect frozen water, although it is included in the scheme). This is subject to the transport equation:

$$\frac{dM_n}{dt} = W_{n-1} - W_n - E_n, \quad (\text{A2})$$

where subscript n denotes the layer, W_n and W_{n-1} are the diffusion terms in the layer and that immediately below it, and E_n is the evapotranspiration (including interaction with roots). The evapotranspiration function

is controlled by land usage and vegetation data embedded in JULES, whereas the diffusion terms are prescribed by the Darcy equation:

$$W = K \left(\frac{\partial \Psi}{\partial z} + 1 \right), \quad (\text{A3})$$

where K is the hydraulic conductivity and Ψ is the soil water suction function. Within MOSES these are respectively described by the Clapp–Hornberger relationships (Clapp and Hornberger 1978):

$$\Psi = \Psi_s S_u^{-b} \quad \text{and} \quad (\text{A4})$$

$$K = K_s S_u^{2b+3}, \quad (\text{A5})$$

where Ψ_s , K_s , and b are empirical constants that can be set on model initialization. For this study, the default values used operationally by the Met Office were used.

There are then two boundary conditions: at the surface, the flux (aside from evaporation) is computed as the summation of canopy throughfall, snowmelt, and surface runoff; underneath the bottom (N th) layer, the drainage (W_N) is set to equal the hydraulic conductivity.

Finally, the evaporation to the atmosphere from soil at the surface is given by

$$E = \rho C_H U_1 [q_{\text{sat}}(T_\star, p_\star) - q_1] \left[f_a + (1 - f_a) \frac{g_s}{g_s + C_H U_1} \right], \quad (\text{A6})$$

where f_a is the tile saturation fraction (e.g., 1 for ice, lake, and ocean and 0 for dry rock), ρ is the density of air, g_s is the surface soil conductivity, U is the wind speed, C_H is the surface flux heat exchange coefficient, q is specific humidity; and the subscripts \star , 1, and sat refer to the surface, lowest atmospheric model level, and saturation respectively.

REFERENCES

- Andersen, T., and M. Shepherd, 2017: Inland tropical cyclones and the “brown ocean” concept. *Hurricanes and Climate Change*, J. M. Collins and K. Walsh, Eds., Springer, 117–134, doi:[10.1007/978-3-319-47594-3_5](https://doi.org/10.1007/978-3-319-47594-3_5).
- Baisya, H., S. Pattnaik, and P. V. Rajesh, 2017: Land surface–precipitation feedback analysis for a landfaling monsoon depression in the Indian region. *J. Adv. Model. Earth Syst.*, **9**, 712–726, doi:[10.1002/2016MS000829](https://doi.org/10.1002/2016MS000829).
- Best, M. J., and Coauthors, 2011: The Joint UK Land Environment Simulator (JULES), model description—Part 1: Energy and water fluxes. *Geosci. Model Dev.*, **4**, 677–699, doi:[10.5194/gmd-4-677-2011](https://doi.org/10.5194/gmd-4-677-2011).
- Bishop, C. H., B. J. Etherton, and S. J. Majumdar, 2001: Adaptive sampling with the ensemble transform Kalman filter. Part I: Theoretical aspects. *Mon. Wea. Rev.*, **129**, 420–436, doi:[10.1175/1520-0493\(2001\)129<0420:ASWTET>2.0.CO;2](https://doi.org/10.1175/1520-0493(2001)129<0420:ASWTET>2.0.CO;2).

- Boos, W. R., J. V. Hurley, and V. S. Murthy, 2015: Adiabatic westward drift of Indian monsoon depressions. *Quart. J. Roy. Meteor. Soc.*, **141**, 1035–1048, doi:[10.1002/qj.2454](https://doi.org/10.1002/qj.2454).
- Bowler, N. E., A. Arribas, K. R. Mylne, K. B. Robertson, and S. E. Beare, 2008: The MOGREPS short-range ensemble prediction system. *Quart. J. Roy. Meteor. Soc.*, **134**, 703–722, doi:[10.1002/qj.234](https://doi.org/10.1002/qj.234).
- Buizza, R., M. Miller, and T. N. Palmer, 1999: Stochastic representation of model uncertainties in the ECMWF ensemble prediction system. *Quart. J. Roy. Meteor. Soc.*, **125**, 2887–2908, doi:[10.1002/qj.49712556006](https://doi.org/10.1002/qj.49712556006).
- Chang, H. I., D. Niyogi, A. Kumar, C. M. Kishtawal, J. Dudhia, F. Chen, U. C. Mohanty, and M. Shepherd, 2009: Possible relation between land surface feedback and the post-landfall structure of monsoon depressions. *Geophys. Res. Lett.*, **36**, L15826, doi:[10.1029/2009GL037781](https://doi.org/10.1029/2009GL037781).
- Charney, J. G., and A. Eliassen, 1964: On the growth of the hurricane depression. *J. Atmos. Sci.*, **21**, 68–75, doi:[10.1175/1520-0469\(1964\)021<0068:OTGOTH>2.0.CO;2](https://doi.org/10.1175/1520-0469(1964)021<0068:OTGOTH>2.0.CO;2).
- Chen, T.-C., J.-H. Yoon, and S.-Y. Wang, 2005: Westward propagation of the Indian monsoon depression. *Tellus*, **57A**, 758–769, doi:[10.3402/tellusa.v57i5.14733](https://doi.org/10.3402/tellusa.v57i5.14733).
- Clapp, R. B., and G. M. Hornberger, 1978: Empirical equations for some soil hydraulic properties. *Water Resour. Res.*, **14**, 601–604, doi:[10.1029/WR014i004p00601](https://doi.org/10.1029/WR014i004p00601).
- Clark, C. A., and R. W. Arritt, 1995: Numerical simulations of the effect of soil moisture and vegetation cover on the development of deep convection. *J. Appl. Meteor.*, **34**, 2029–2045, doi:[10.1175/1520-0450\(1995\)034<2029:NSOTEO>2.0.CO;2](https://doi.org/10.1175/1520-0450(1995)034<2029:NSOTEO>2.0.CO;2).
- Cohen, N. Y., and W. R. Boos, 2016: Perspectives on moist baroclinic instability: Implications for the growth of monsoon depressions. *J. Atmos. Sci.*, **73**, 1767–1788, doi:[10.1175/JAS-D-15-0254.1](https://doi.org/10.1175/JAS-D-15-0254.1).
- Cox, P. M., R. A. Betts, C. B. Bunton, R. L. H. Essery, P. R. Rowntree, and J. Smith, 1999: The impact of new land surface physics on the GCM simulation of climate and climate sensitivity. *Climate Dyn.*, **15**, 183–203, doi:[10.1007/s003820050276](https://doi.org/10.1007/s003820050276).
- Craig, G. C., and S. L. Gray, 1996: CISK or WISHE as the mechanism for tropical cyclone intensification. *J. Atmos. Sci.*, **53**, 3528–3540, doi:[10.1175/1520-0469\(1996\)053<3528:COWATM>2.0.CO;2](https://doi.org/10.1175/1520-0469(1996)053<3528:COWATM>2.0.CO;2).
- Davies, T., M. J. P. Cullen, A. J. Malcolm, M. H. Mawson, A. Staniforth, A. A. White, and N. Wood, 2005: A new dynamical core for the Met Office's global and regional modelling of the atmosphere. *Quart. J. Roy. Meteor. Soc.*, **131**, 1759–1782, doi:[10.1256/qj.04.101](https://doi.org/10.1256/qj.04.101).
- Dee, D. P., and Coauthors, 2011: The ERA-Interim reanalysis: Configuration and performance of the data assimilation system. *Quart. J. Roy. Meteor. Soc.*, **137**, 553–597, doi:[10.1002/qj.828](https://doi.org/10.1002/qj.828).
- Edwards, J. M., and A. Slingo, 1996: Studies with a flexible new radiation code. I: Choosing a configuration for a large-scale model. *Quart. J. Roy. Meteor. Soc.*, **122**, 689–719, doi:[10.1002/qj.49712253107](https://doi.org/10.1002/qj.49712253107).
- Eltahir, E. A. B., 1998: A soil moisture–rainfall feedback mechanism: 1. Theory and observations. *Water Resour. Res.*, **34**, 765–776, doi:[10.1029/97WR03499](https://doi.org/10.1029/97WR03499).
- Essery, R. L. H., M. J. Best, R. A. Betts, P. M. Cox, and C. M. Taylor, 2003: Explicit representation of subgrid heterogeneity in a GCM land surface scheme. *J. Hydrometeorol.*, **4**, 530–543, doi:[10.1175/1525-7541\(2003\)004<0530:EROSHI>2.0.CO;2](https://doi.org/10.1175/1525-7541(2003)004<0530:EROSHI>2.0.CO;2).
- Fan, Y., and H. van den Dool, 2004: Climate Prediction Center global monthly soil moisture data set at 0.5 degree resolution for 1948 to present. *J. Geophys. Res.*, **109**, D10102, doi:[10.1029/2003JD004345](https://doi.org/10.1029/2003JD004345).
- Godbole, R. V., 1977: The composite structure of the monsoon depression. *Tellus*, **29**, 25–40, doi:[10.3402/tellusa.v29i1.11327](https://doi.org/10.3402/tellusa.v29i1.11327).
- Gregory, D., and P. R. Rowntree, 1990: A mass flux convection scheme with representation of cloud ensemble characteristics and stability-dependent closure. *Mon. Wea. Rev.*, **118**, 1483–1506, doi:[10.1175/1520-0493\(1990\)118<1483:AMFCSW>2.0.CO;2](https://doi.org/10.1175/1520-0493(1990)118<1483:AMFCSW>2.0.CO;2).
- Holton, J. R., and G. J. Hakim, 2013: *An Introduction to Dynamic Meteorology*. International Geophysics Series, Vol. 88, Academic Press, 532 pp.
- Hotelling, H., 1992: The generalization of Student's ratio. *Breakthroughs in Statistics*, S. Kotz and N. L. Johnson, Eds., Springer, 54–65, doi:[10.1007/978-1-4612-0919-5_4](https://doi.org/10.1007/978-1-4612-0919-5_4).
- Huffman, G. J., R. F. Adler, D. T. Bolvin, and E. J. Nelkin, 2010: The TRMM multi-satellite precipitation analysis (TMPA). *Satellite Rainfall Applications for Surface Hydrology*, M. Gebremichael and F. Hossain, Eds., Springer, 3–22.
- Hunt, K. M. R., and D. J. Parker, 2016: The movement of Indian monsoon depressions by interaction with image vortices near the Himalayan wall. *Quart. J. Roy. Meteor. Soc.*, **142**, 2224–2229, doi:[10.1002/qj.2812](https://doi.org/10.1002/qj.2812).
- , A. G. Turner, P. M. Inness, D. E. Parker, and R. C. Levine, 2016a: On the structure and dynamics of Indian monsoon depressions. *Mon. Wea. Rev.*, **144**, 3391–3416, doi:[10.1175/MWR-D-15-0138.1](https://doi.org/10.1175/MWR-D-15-0138.1).
- , —, and D. E. Parker, 2016b: The spatiotemporal structure of precipitation in Indian monsoon depressions. *Quart. J. Roy. Meteor. Soc.*, **142**, 3195–3210, doi:[10.1002/qj.2901](https://doi.org/10.1002/qj.2901).
- Hurley, J. V., and W. R. Boos, 2015: A global climatology of monsoon low pressure systems. *Quart. J. Roy. Meteor. Soc.*, **141**, 1049–1064, doi:[10.1002/qj.2447](https://doi.org/10.1002/qj.2447).
- Kellner, O., D. Niyogi, M. Lei, and A. Kumar, 2012: The role of anomalous soil moisture on the inland reintensification of Tropical Storm Erin (2007). *Nat. Hazards*, **63**, 1573–1600, doi:[10.1007/s11069-011-9966-6](https://doi.org/10.1007/s11069-011-9966-6).
- Kishtawal, C., D. Niyogi, B. Rajagopalan, M. Rajeevan, N. Jaiswal, and U. Mohanty, 2013: Enhancement of inland penetration of monsoon depressions in the Bay of Bengal due to prestorm ground wetness. *Water Resour. Res.*, **49**, 3589–3600, doi:[10.1002/wrcr.20301](https://doi.org/10.1002/wrcr.20301).
- Krishnamurthy, V., and J. Shukla, 2007: Intraseasonal and seasonally persisting patterns of Indian monsoon rainfall. *J. Climate*, **20**, 3–20, doi:[10.1175/JCLI3981.1](https://doi.org/10.1175/JCLI3981.1).
- , and R. S. Ajayamohan, 2010: Composite structure of monsoon low pressure systems and its relation to Indian rainfall. *J. Climate*, **23**, 4285–4305, doi:[10.1175/2010JCLI2953.1](https://doi.org/10.1175/2010JCLI2953.1).
- Kummerow, C., W. Barnes, T. Kozu, J. Shiue, and J. Simpson, 1998: The Tropical Rainfall Measuring Mission (TRMM) sensor package. *J. Atmos. Oceanic Technol.*, **15**, 809–817, doi:[10.1175/1520-0426\(1998\)015<0809:TTRMMT>2.0.CO;2](https://doi.org/10.1175/1520-0426(1998)015<0809:TTRMMT>2.0.CO;2).
- Liu, Y.-Y., R. Parinussa, W. A. Dorigo, R. A. M. De Jeu, W. Wagner, A. I. J. M. van Dijk, M. F. McCabe, and J. P. Evans, 2011: Developing an improved soil moisture dataset by blending passive and active microwave satellite-based retrievals. *Hydrol. Earth Syst. Sci.*, **15**, 425–436, doi:[10.5194/hess-15-425-2011](https://doi.org/10.5194/hess-15-425-2011).
- , W. A. Dorigo, R. M. Parinussa, R. A. M. de Jeu, W. Wagner, M. F. McCabe, J. P. Evans, and A. I. J. M. van Dijk, 2012: Trend-preserving blending of passive and active microwave soil moisture retrievals. *Remote Sens. Environ.*, **123**, 280–297, doi:[10.1016/j.rse.2012.03.014](https://doi.org/10.1016/j.rse.2012.03.014).

- Mooley, D. A., 1980: Severe cyclonic storms in the Bay of Bengal, 1877–1977. *Mon. Wea. Rev.*, **108**, 1647–1655, doi:[10.1175/1520-0493\(1980\)108<1647:SCSITB>2.0.CO;2](https://doi.org/10.1175/1520-0493(1980)108<1647:SCSITB>2.0.CO;2).
- Rajesh, P. V., and S. Pattnaik, 2016: High resolution land surface response of inland moving Indian monsoon depressions over Bay of Bengal. *Remote Sensing and Modeling of the Atmosphere, Oceans, and Interactions VI*, T. N. Krishnamurti and M. N. Rajeevan, Eds., International Society for Optics and Photonics (SPIE Proceedings, Vol. 9882), 98820K, doi:[10.1117/12.2239712](https://doi.org/10.1117/12.2239712).
- Ramanathan, K. R., and K. P. Ramakrishnan, 1933: The Indian southwest monsoon and the structure of depressions associated with it. *Mem. Indian Meteor. Dept.*, **26**, 13–36.
- Rao, K. N., and S. Jayamaran, 1958: A statistical study of frequency of depressions and cyclones in the Bay of Bengal. *Indian J. Meteor. Geophys.*, **9**, 187–194.
- Roy, P. S., and Coauthors, 2015: Development of decadal (1985–1995–2005) land use and land cover database for India. *Remote Sens.*, **7**, 2401–2430, doi:[10.3390/rs70302401](https://doi.org/10.3390/rs70302401).
- Shukla, J., 1978: CISK-barotropic-baroclinic instability and the growth of monsoon depressions. *J. Atmos. Sci.*, **35**, 495–508, doi:[10.1175/1520-0469\(1978\)035<0495:CBBIAT>2.0.CO;2](https://doi.org/10.1175/1520-0469(1978)035<0495:CBBIAT>2.0.CO;2).
- Shutts, G., 2005: A kinetic energy backscatter algorithm for use in ensemble prediction systems. *Quart. J. Roy. Meteor. Soc.*, **131**, 3079–3102, doi:[10.1256/qj.04.106](https://doi.org/10.1256/qj.04.106).
- Van den Dool, H., J. Huang, and Y. Fan, 2003: Performance and analysis of the constructed analogue method applied to us soil moisture over 1981–2001. *J. Geophys. Res.*, **108**, 8617, doi:[10.1029/2002JD003114](https://doi.org/10.1029/2002JD003114).
- Vinodkumar, A. Chandrasekar, K. Alapathy, and D. S. Niyogi, 2007: The effect of a surface data assimilation technique and the traditional four-dimensional data assimilation on the simulation of a monsoon depression over India using a mesoscale model. *Nat. Hazards*, **42**, 439–453, doi:[10.1007/s11069-006-9080-3](https://doi.org/10.1007/s11069-006-9080-3).
- , ———, and D. Niyogi, 2008: The impacts of indirect soil moisture assimilation and direct surface temperature and humidity assimilation on a mesoscale model simulation of an Indian monsoon depression. *J. Appl. Meteor. Climatol.*, **47**, 1393–1412, doi:[10.1175/2007JAMC1599.1](https://doi.org/10.1175/2007JAMC1599.1).
- Wagner, W., W. Dorigo, R. de Jeu, D. Fernandez, J. Benveniste, E. Haas, and M. Ertl, 2012: Fusion of active and passive microwave observations to create an essential climate variable data record on soil moisture. *Proc. XXII Int. Society for Photogrammetry and Remote Sensing (ISPRS) Congress*, Vol. 25, Melbourne, Australia, ISPRS, 315–321.
- Walters, D., and Coauthors, 2017: The Met Office Unified Model Global Atmosphere 6.0/6.1 and JULES Global Land 6.0/6.1 configurations. *Geosci. Model Dev.*, **10**, 1487–1520, doi:[10.5194/gmd-10-1487-2017](https://doi.org/10.5194/gmd-10-1487-2017).
- Welch, B. L., 1947: The generalization of Student's problem when several different population variances are involved. *Biometrika*, **34**, 28–35, doi:[10.2307/2332510](https://doi.org/10.2307/2332510).
- Wilson, D. R., A. C. Bushell, A. M. Kerr-Munslow, J. D. Price, and C. J. Morcrette, 2008: PC2: A prognostic cloud fraction and condensation scheme. I: Scheme description. *Quart. J. Roy. Meteor. Soc.*, **134**, 2093–2107, doi:[10.1002/qj.333](https://doi.org/10.1002/qj.333).